RSC Advances

Large Micro-Sized K2TiF6:Mn4+ Red Phosphors Synthesised by a Simple Reduction Reaction for High Colour-Rendering White Light-Emitting Diodes

Journal:	*RSC Advances*
Manuscript ID	RA-ART-08-2015-016709.R3
Article Type:	Paper
Date Submitted by the Author:	11-Nov-2015
Complete List of Authors:	Han, Tao; Chongqing University of Arts and Sciences, Lang, Tianchun; Chongqing University of Arts and Sciences, Wang, Jun; Chongqing University of Arts and Sciences, Tu, Ming-jing; Chongqing University of Arts and Sciences, ; Sichuan University, Peng, Lingling; Chongqing University of Arts and Sciences,
Subject area & keyword:	Optical materials < Materials

Journal Name

ARTICLE

Large Micro-Sized $K_2TiF_6:Mn^{4+}$ Red Phosphors Synthesised by a Simple Reduction Reaction for High Colour-Rendering White Light-Emitting Diodes

Received 00th January 20xx,
Accepted 00th January 20xx

DOI: 10.1039/x0xx00000x

www.rsc.org/

Tao Han[a], Tianchun Lang[a], Jun Wang[a], Mingjing Tu[a] and Lingling Peng[a]

A simple chemical method for synthesising large micro-sized $K_2TiF_6:Mn^{4+}$ phosphors (50-100 μm) is presented, based on a direct reduction reaction with K_2TiF_6 particles immersed in $KMnO_4$/HF solution. The Mn^{4+} concentration in K_2TiF_6 primarily increases as the initial $KMnO_4$ concentration is increased, subject to the diffusion of Mn^{4+} ions. However, the relative emission intensity of our synthesised $K_2TiF_6:Mn^{4+}$ is first enhanced and then declines with increasing $KMnO_4$ concentration, with an optimum $KMnO_4$ concentration of 0.016 g/ml, which most likely depends on the concentration quenching effect. The synthesised $K_2TiF_6:Mn^{4+}$ (0.35- 4.4 at.%) phosphors show good thermal stability and can be adopted to fabricate high CRI (Ra＞85) white LEDs for indoor lighting.

1. Introduction

Solid state lighting based on light-emitting diodes (LEDs) will replace all incandescent bulbs and compact fluorescent lamps, due to their energy-saving, environmentally friendly, and long-lasting features.[1, 2] Until now, an InGaN chip (emitting near 460 nm) combined with a yellow $Y_3Al_5O_{12}:Ce^{3+}$ phosphor has been the most mature method for fabricating commercial white LEDs. However, the low colour-rendering index (CRI, Ra＜80) and high correlated colour temperature (CCT, ~6000 K), caused by the lack of a red light component in the spectral region of the $Y_3Al_5O_{12}:Ce^{3+}$ phosphor, limit the use of this approach in some important applications, such as indoor lighting.[3] One strategy adopted to resolve the issue is the use of a red-emitting material (e.g., $Sr_2Si_5N_8:Eu^{2+}$ or $CaAlSiN_3:Eu^{2+}$) blended with a yellow phosphor. The solution can produce warm-white light (CCT=2840 K) and a sufficiently high CRI (Ra=80-96).[4, 5] However, these red nitride phosphors cause serious re-absorption, thus reducing the luminous efficacy, when mixed with a yellow phosphor. Additionally, the rigorous synthesis conditions required for nitride compounds present another drawback.

Recently, some Mn^{4+}-activated fluoride phosphors in the form of A_2MF_6 (A=Na, K, Rb, Cs, NH^{4+}; M=Ti, Ge, Si, Sn, Ga, Y) or BMF_6 (B= Mg, Ca, Ba, Sr, Zn; M=Ti, Ge, Si)[6-13] have been shown to exhibit efficient red emission under blue or UV excitation and may be promising candidates for blue-chip excited white LEDs with a high CRI, low CCT, high luminous efficacy and high quenching temperatures.[14] By employing $K_2TiF_6:Mn^{4+}$ as a red phosphor, Zhu et al.[15] fabricated a high-performance white LED with a low CCT (3556 K), a high CRI (Ra=81) and a luminous efficacy of 116 lm/W. $K_2TiF_6:Mn^{4+}$ phosphors are usually prepared by cocrystallisation[16], chemical etching[17] or cation exchange[18]. Of these methods, cation exchange is a general but efficient synthesis method, based on cation (Ti^{4+} and Mn^{4+}) exchange from K_2TiF_6 (Ti^{4+} source host) and K_2MnF_6 (Mn^{4+} source materials). In these synthesis procedures, Mn^{4+} is always derived from $KMnO_4$ (Mn^{7+}) via a reduction reaction; thus, it is possible to propose a simpler method for synthesising highly efficient $K_2TiF_6:Mn^{4+}$ phosphors using $KMnO_4$ as a direct reactant.

Here, we report a simple reduction reaction for synthesising large micro-sized $K_2TiF_6:Mn^{4+}$ red phosphors. We demonstrate that the Mn^{4+} concentrations in the K_2TiF_6 host are 3.7-5.3 at.% (approximately 50 at.% Mn^{7+} reduced to Mn^{4+}) and that the emission spectrum of the obtained $K_2TiF_6:Mn^{4+}$ consists of five narrow bands, extending from 580 to 660 nm, with the strongest peak at 634.8 nm (~2 eV). Upon the addition of the synthesised $K_2TiF_6:Mn^{4+}$, the fabricated white LED exhibits a high CRI (Ra＞85) and is thus suitable for indoor lighting.

2. Experimental

K_2TiF_6 (AR), $KMnO_4$ (AR), $KF{\cdot}2H_2O$ (AR), HF solution (≥40 wt.%, AR) and H_2O_2 solution (≥30 wt.%, AR) were purchased from the Tianjin Yongda Chemical Reagent Company, Limited, China. All of the chemicals were used directly without further purification. $K_2TiF_6:Mn^{4+}$ phosphors were synthesised by a simple reduction reaction. Typically, a certain amount of $KMnO_4$ powder and $KF{\cdot}2H_2O$ crystals were combined in 5 ml of HF solution, and then, 3.0 g of K_2TiF_6 particles was added to form a purple mixture. Next, 10 wt.% H_2O_2 solution was slowly dropped into the obtained purple mixture under stirring. Finally, the products were separated by vacuum filtration and rinsed in 10 wt.% HF solution and ethanol.

[a]Chongqing Engineering Research Center for Optoelectronic Materials and Devices, Research Institute for New Materials Technology, Chongqing University of Arts and Sciences, Chongqing 402160, People's Republic of China. E-mail: danbaiht@126.com; Tel.: +86 02349891750; Fax.: +86 02349891750.

†Electronic Supplementary Information (ESI) available. See DOI: 10.1039/x0xx00000x

The crystalline structures of the samples were analysed using an X-ray diffractometer (XRD-6000, Shimadzu) with Cu Kα1 radiation (λ=0.154187 nm). Powder XRD data were collected in scanning mode for a 2θ range of 10° to 80° with a step of 0.02° and a rate of 2.0° min^{-1}. Unit cell refinements were accomplished using JADE software. The morphologies of the samples were acquired using a scanning electron microscope (Quanta 250, FEI) with an accelerating voltage of 10 kV. X-ray photoelectron spectra (XPS) were collected using an electron spectrometer (V4105, Thermo Electron).

The chemical element analyses present in the materials at the microscopic level were performed by energy dispersive X-ray spectrometry (Apollo XLT, EDAX) in conjunction with scanning electron microscopy and compositional quantitative analyses were performed using an inductively coupled plasma optical emission spectrometry (ICP–OES) (OPTIMA 2000DV, Perkin Elmer). The photoluminescence properties of the samples were measured by a fluorescence spectrophotometer (F-7000, Hitachi) with a 150-W xenon lamp as the excitation source. The quantum efficiencies were measured by the F-7000 fluorescence spectrophotometer equipped with an integrating sphere at the room temperature. In the determination, the samples were placed in a metal cell, and then absorption spectrum of $BaSO_4$ white reflectance standard sample, absorption spectrum of samples, and emission spectrum of samples were obtained, respectively. The internal (external) quantum efficiency was calculated by QuantumYields tool with the ratio of the number of photons in the emission spectrum to that in the absorption (excitation) spectrum. The temperature quenching property was detected by thermocouples inside the plaque and was controlled with a standard high-temperature fluorescence controller (TAP-02, Orient KOJI). The luminous efficiency, colour-rendering index, and the Commission Internationale de l'Eclairage (CIE) colour coordinates of the fabricated LEDs were characterised using a high-accuracy LED photo-colour and electron test system (HSP3000, Hangzhou Hongpu Optoelectronics Technology Co. Ltd., China) and were evaluated under a current of 90 mA.

3. Results and discussion

According to the literature,[15, 18, 19] the cation exchange reaction is a convenient method for preparing Mn^{4+}-activated fluoride phosphors. However, the main difficulty in synthesising Mn^{4+}-activated fluoride compounds lies in the diverse valence states of Mn, including Mn^{2+}, Mn^{3+}, and Mn^{5+}. Of these, Mn^{2+}-activated fluoride phosphors measured by excitation at 325 nm reveal a single broad emission peak at ~585 nm ($^4T_1 \rightarrow {}^6A_1$),[20] and Mn^{5+}-doped crystals exhibit optical absorption in the spectral region from the near IR to UV, with near-IR luminescence observed at ~1100 – 1300 nm at very low intensities.[21] In addition, the Mn^{3+} ion is not an efficient activator in most host insulators.[22]

K_2MnF_6 can be synthesised by a simple chemical reaction as follows:

$$2KMnO_4 + 2KF + 10HF + 3H_2O_2 \rightarrow 2K_2MnF_6 + 8H_2O + 3O_2. \quad (1)$$

However, the synthesised fluoride compound is $K_2MnF_5{\cdot}H_2O$ in aqueous solution.[23] Thus, Equation (1) is one of the intermediate reactions in the process for reducing $KMnO_4$ in HF solution by H_2O_2. Based on this fact, we developed a simple method for synthesising K_2TiF_6:Mn^{4+}. The synthesis was performed by mixing $KMnO_4$, $KF{\cdot}2H_2O$ and K_2TiF_6 in HF solution, with H_2O_2 as a reducing agent, added dropwise. The synthesis process and reaction mechanism are illustrated in Figure 1. Figure 1a-c shows the colour changes of the mixture during the reducing process. The colour of the initial mixture is dark purple, due to the $KMnO_4$ solution, and the colour of the final mixture is brown, due to the secondary colours of the products and the Mn coordination compound solution. The brown mixture was filtered, washed and dried; then, orange-yellow products were obtained, which can emit strong red light under blue or UV illumination. As reported in the literature,[24] red-emitting Mn^{4+}-activated fluoride phosphors are known to be yellow or light orange. The following characterisations also demonstrate that the orange-yellow products are K_2TiF_6:Mn^{4+} phosphors. The most likely reaction mechanism (see Figure 1d) is the reduction of Mn^{7+} to Mn^{5+}, Mn^{4+}, Mn^{3+} or Mn^{2+} by H_2O_2, but only Mn^{4+} can replace Ti^{4+} in the K_2TiF_6 host because the Mn^{4+} ion has an effective ion radius of r = 0.53 Å, which is easily substituted for the Ti^{4+} ion (r = 0.61 Å) in the TiF_6^{2-} octahedra, rather than the Mn^{2+} ion (r = 0.83 Å), Mn^{3+} ion (r = 0.65 Å) or Mn^{5+} ion (coordination number = 4, r = 0.33 Å).[25] The replacement of Ti^{4+} in the K_2TiF_6 host with the Mn^{4+} in the solution is a cation exchange reaction, which facilitates the formation of Mn^{4+} in the reduction reaction. In contrast to the traditional procedure, the above synthetic procedure is simplified, and the reduction reaction and cation exchange occur simultaneously to generate mutual promotion.

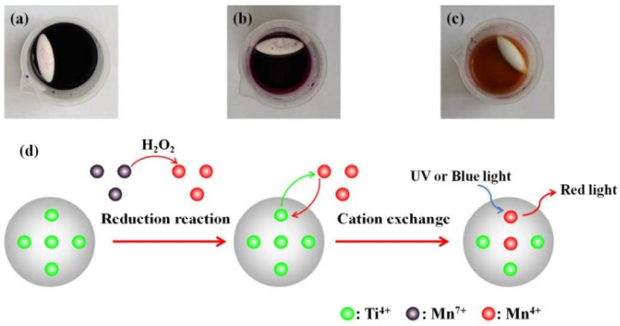

Figure 1. Images of the initial mixture of $KMnO_4$, $KF{\cdot}2H_2O$ and K_2TiF_6 in HF solution (a), the partly reduced mixture (b) and the final mixture (c). (d) Schematic illustration of the reaction mechanism for synthesising K_2TiF_6:Mn^{4+}.

Figures 2a and b present images of the synthesised K_2TiF_6:Mn^{4+} acquired under room light and UV light illumination. The synthesised K_2TiF_6:Mn^{4+} powders appear orange-yellow and emit strong red light under UV light illumination. Figure 2d displays the XPS spectrum of the synthesised samples. The spectrum shape and peak parameter (~ 641.5 eV) coincide with a previous report on Mn^{4+} ion.[26] The Mn^{4+} ion was substituted for the Ti^{4+} ion in the K_2TiF_6 unit cell (see Figure 2c). Figure 3 shows the XRD patterns of the raw K_2TiF_6 materials and the samples synthesised by adding various $KMnO_4$ concentrations. All diffraction peaks are in agreement with the hexagonal K_2TiF_6 phase (JCPDS No. 08-0488). No K_2MnF_6 phase (JCPDS No. 34-0733) and other phase or impurity can be detected. Figure 2c shows a schematic of the crystal structure of the K_2TiF_6 unit cell. In the crystal lattice of K_2TiF_6, Ti^{4+} is

six-coordinated in the TiF_6^{2-} octahedral structure, and the K^+ ion is surrounded by 12 nearest neighbour F^-, forming a three-dimensional framework. No traces of the Mn compound phase or other impurity peaks were observed. Nonetheless, the diffraction peaks of 2θ appear at 19.0°, 38.6° and 42.8°, assigned to the (0 0 1), (0 0 2) and (1 0 2) planes, whose intensities were distinctly weakened. To determine the cause of this result, we compared SEM images of the K_2TiF_6 powders and the synthesised $K_2TiF_6:Mn^{4+}$ (see Figure 4). The K_2TiF_6 particles and the synthesised $K_2TiF_6:Mn^{4+}$ particles have a similar size of 50-100 μm but different morphologies. K_2TiF_6 particles show an irregular disk-like morphology, whereas the synthesised $K_2TiF_6:Mn^{4+}$ particles display two morphologies of a sheet shape and an oblate sphere with a rough surface, resulting from the cation exchange and the HF corrosion. The decrease of the lattice planes in the reaction process leads to the morphology change of the synthesised $K_2TiF_6:Mn^{4+}$ particles. According to the literature,[27] large micro-sized cube phosphors (~100 μm) are scatter-free, and their luminous efficacy and packaging efficiency are higher than those of commercial powder phosphor.

To verify that the Mn^{4+} ions were doped in the K_2TiF_6 host, unit cell refinements of the samples were performed using JADE software, which indicated that the fitted interplanar distance decreased from 2.173 Å for the raw K_2TiF_6 materials to 2.167 Å for the synthesised $K_2TiF_6:Mn^{4+}$ (1.1 at.%). This result is consistent with the expected structural change induced by the substitution of the smaller Mn^{4+} cation for the larger Ti^{4+} cation in the crystalline lattice.

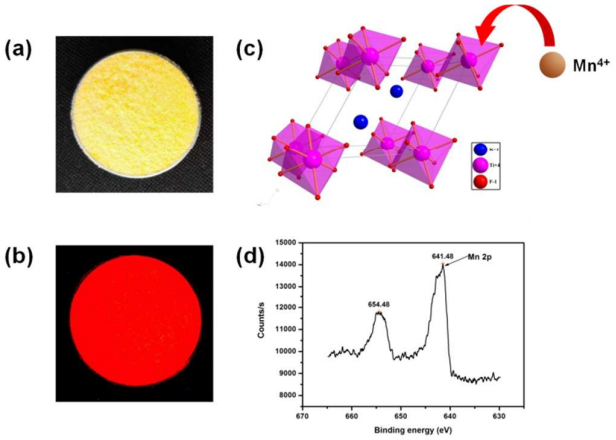

Figure 2. Images of the synthesised $K_2TiF_6:Mn^{4+}$ under room light (a) and UV light illumination (b). (c) Schematic of the crystal structure of a K_2TiF_6 unit cell. (d) XPS spectrum of the synthesised samples.

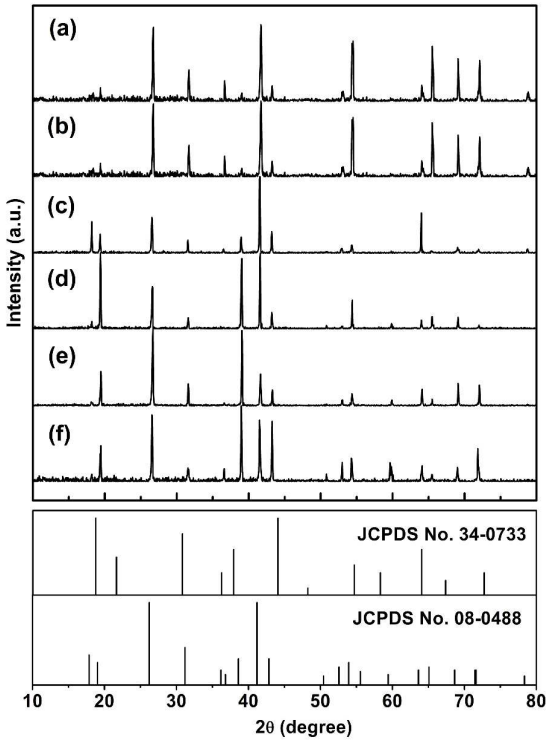

Figure 3. XRD patterns of samples synthesised by adding 0.064, 0.032, 0.021, 0.016, 0.013 g/ml (a-e) $KMnO_4$ and raw K_2TiF_6 materials (f).

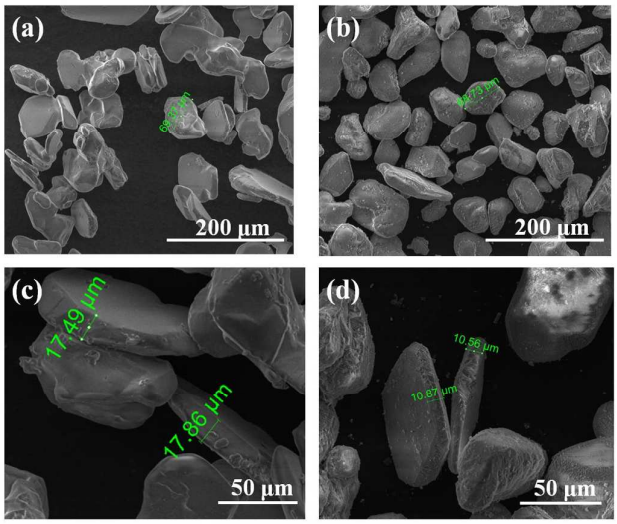

Figure 4. SEM images of K_2TiF_6 powders (a, c) and the synthesised $K_2TiF_6:Mn^{4+}$ (1.1 at.%) phosphors (b, d).

In the present work, the cation exchange procedure is a solid-liquid reaction, in which the diffusion of the Mn^{4+} ion plays an important role. On the basis of Fick's law, the diffusion flux is proportional to its concentration gradient, so the initial concentration of $KMnO_4$ in the HF solution should have a strong effect on the Mn^{4+} doping percentage and the photoluminescence properties of the final products. The Mn^{4+} doping percentage in K_2TiF_6 was estimated from the EDX results (see Figure 5). All energy peaks correspond to the elements in $K_2TiF_6:Mn^{4+}$, except for the

peaks at 0.25 and 0.5 keV, which correspond to organic matter from the preparation process. ICP–OES analyses reveal that the Mn^{4+} concentrations of the samples are 0.35- 4.4 at.% (approximately 50 at.% Mn^{7+} reduced to Mn^{4+}) and increase with an increasing initial $KMnO_4$ concentration. Monitored at 460 nm excitation, the synthesised K_2TiF_6:Mn^{4+} (1.1 at.%) shows a high internal quantum efficiency of 0.825 and an external quantum efficiency of 0.568, respectively.

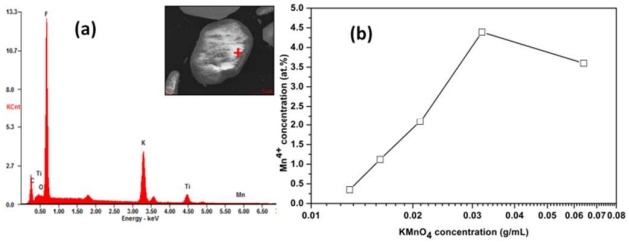

Figure 5. EDX spectrum (a) of the synthesised K_2TiF_6:Mn^{4+} (1.1 at.%) and the dependence (b) of the Mn^{4+} concentration (at.%) on the initial $KMnO_4$ concentration.

Mn^{4+} ($3d^3$ configuration) in the crystalline host produces a strong crystal field due to its high effective positive charge. Therefore, the emission spectra of many Mn^{4+}-activated red phosphors are dominated by the spin-forbidden $^2E_g \rightarrow {}^4A_{2g}$ transition (sharp line), such as Na_2SiF_6:Mn^{4+}, Cs_2GeF_6:Mn^{4+}, $SrTiO_3$:Mn^{4+}, $YAlO_3$:Mn^{4+}, and $Y_2Sn_2O_7$:Mn^{4+}.[28, 29] The emission spectrum of the synthesised K_2TiF_6:Mn^{4+} consists of five narrow bands, extending from 580 to 660 nm, with the strongest peak at 634.8 nm (~2 eV) (see Figure 6b), assigned to the $^2E_g \rightarrow {}^4A_{2g}$ transition. Because the energy of the ^2E_g state in the d^3 electronic configuration is independent of the crystal field (as demonstrated by Tanabe–Sugano diagrams), the increased width of the emission lines is not due to variations in the crystal field strength but can be explained by the strong electron–vibrational interaction between the electronic states of the Mn^{4+} ions and crystal lattice vibrations. The two broad excitation bands peaking at ~365 nm (~3.5 eV) and ~460 nm (~2.7 eV) are attributed to the $^4A_{2g} \rightarrow {}^4T_{2g}$ and $^4A_{2g}$-$^4T_{1g}$ spin-allowed transitions (see Figure 6a). The emission and excitation spectra of our synthesised K_2TiF_6:Mn^{4+} differ from those of $CaAlN_3$:Eu^{2+} red phosphors (see Figure 6a). The excitation bands of our synthesised K_2TiF_6:Mn^{4+}, with peaks at ~460 nm, are more suitable for blue LED chips, and their emission bands fit well with the sensitivity curve of photopic human vision due to the lower emission beyond 650 nm, a range in which the human eye is insensitive.[30] The Mn^{4+} in K_2TiF_6:Mn^{4+} comes from the initial $KMnO_4$, which thus has an important influence on the relative emission intensity of the synthesised K_2TiF_6:Mn^{4+} phosphor (see Figure 7). The relative emission intensity of the sample first increases and then declines as the $KMnO_4$ concentration is increased, depending on the concentration quenching effect of the Mn^{4+} activator. The optimum $KMnO_4$ concentration is 0.016 g/ml. The intensity of K_2TiF_6:Mn^{4+} synthesised by a slow titration reaction is much greater than that obtained by a quick reaction due to the effect of the diffusion time.

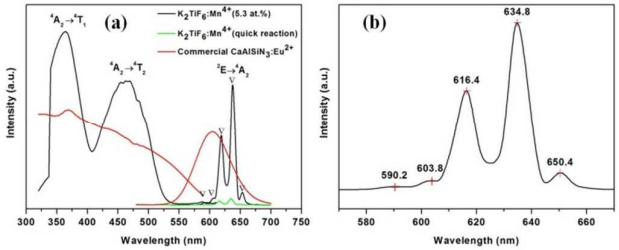

Figure 6. Excitation spectra (λ_{em}=635 nm) and emission spectra (λ_{ex}=460 nm) of the synthesised samples and commercial red phosphors (a) and the emission spectrum of the synthesised K_2TiF_6:Mn^{4+} (4.4 at.%).

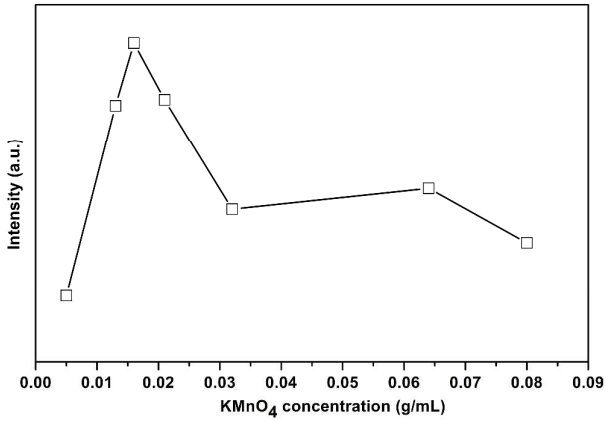

Figure 7. Dependence of the relative emission intensity of the synthesised K_2TiF_6:Mn^{4+} based on the initial $KMnO_4$ concentration.

The thermal stability of a phosphor is an important issue for the application of white LEDs because it affects the chromaticity and brightness of the white light output. Figure 8a shows the temperature dependence of the photoluminescence properties for the synthesised K_2TiF_6:Mn^{4+} (1.1 at.%). The relative photoluminescence intensity of the sample decreases with increasing temperature over the range of 25 to 250 ℃ due to the larger non-radiative transition probability at higher temperatures. The activation energy (ΔE) was calculated by the Arrhenius equation:[31]

$$I(T) \approx \frac{I_0}{1 + A\exp(-\frac{\Delta E}{kT})} \quad (2)$$

where I_0 and I are the photoluminescence intensities of the synthesised K_2TiF_6:Mn^{4+} at room temperature (25 ℃) and the testing temperature, respectively; A is constant and does not influence the calculation; and k is Boltzmann's constant (8.617×10^{-5} eV/K). Figure 8b presents a plot of ln (I_0/I-1) against 1/kT (b) for the synthesised K_2TiF_6:Mn^{4+} (1.1 at.%), fitted to the thermal quenching data. The estimated value of ΔE was 0.34 eV, which is higher than that of nitride compounds (~0.25 eV),[32] indicating better thermal stability.

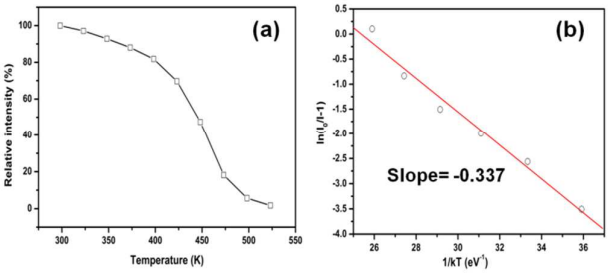

Figure 8. Temperature-dependent photoluminescence properties (a) and plot of ln (I_0/I-1) against 1/kT (b) of the synthesised K_2TiF_6:Mn^{4+} (1.1 at.%).

To demonstrate the application of the synthesised K_2TiF_6:Mn^{4+} red phosphors, white LEDs were fabricated with different phosphors and blue chips (455 nm). Figure 9 shows CIE chromaticity diagrams of the fabricated white LEDs under a drive current of 20 mA. By tuning the weight ratio of the synthesised K_2TiF_6:Mn^{4+} red phosphors to the yellow $Y_3Al_5O_{12}$:Ce^{3+} phosphors, the chromaticity coordinates (x, y) of the LEDs vary from the white light (0.344, 0.322) to the warm-white light (x=0.434, y=0.372) region, which is broader than the region for LEDs fabricated with only $Y_3Al_5O_{12}$:Ce^{3+} phosphors. Table 1 compares relevant photoelectric parameters, such as the CCT, CRI and luminous efficacy, for the fabricated LEDs. The LED fabricated by combining a blue chip and a blend of K_2TiF_6:Mn^{4+} red phosphor and $Y_3Al_5O_{12}$:Ce^{3+} phosphor exhibited a lower CCT and a higher CRI than the LED with only the $Y_3Al_5O_{12}$:Ce^{3+} phosphor due to the additional red light component in the emission spectrum of the LED, which can be confirmed by the electroluminescence spectra (see Figure 9b). After adding the synthesised K_2TiF_6:Mn^{4+}, the white LED has a high CRI (Ra＞85), which is suitable for indoor lighting. Moreover, the luminous efficacy of the white LED with the synthesised K_2TiF_6:Mn^{4+} remains almost the same, although the yellow component of its spectrum weakens due to the decreased amount of $Y_3Al_5O_{12}$:Ce^{3+} phosphor.

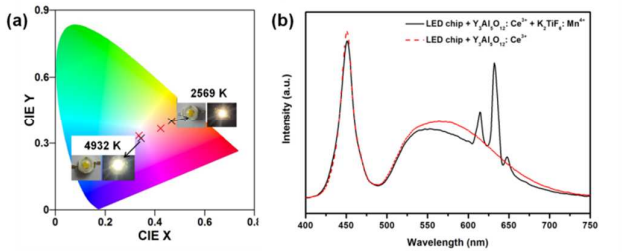

Figure 9. (a) CIE chromaticity diagrams of white LEDs fabricated with blue chips, yellow $Y_3Al_5O_{12}$:Ce^{3+} phosphors and the synthesised K_2TiF_6:Mn^{4+} red phosphors (black cross) in comparison to the yellow $Y_3Al_5O_{12}$:Ce^{3+} phosphors alone (red cross) under a drive current of 20 mA. Inset: Images of the white LEDs with different correlated colour temperatures (CCTs) fabricated with blue chips, yellow $Y_3Al_5O_{12}$:Ce^{3+} phosphors and the synthesised K_2TiF_6:Mn^{4+} red phosphors. (b) Electroluminescence spectra of the fabricated white LEDs.

4. Conclusions

On the basis of the reduction reaction of $KMnO_4$ (Mn^{7+}) to Mn^{4+}, we synthesised K_2TiF_6:Mn^{4+} phosphors by a simple chemical reaction using K_2TiF_6 particles immersed in $KMnO_4$/HF solution. The obtained K_2TiF_6:Mn^{4+} phosphors have a size of 50-100 μm. The Mn^{4+} concentrations in the K_2TiF_6 host are 0.35- 4.4 at.% (approximately 50 at.% Mn^{7+} reduced to Mn^{4+}). The Mn^{4+} concentration in K_2TiF_6 increases with increasing initial $KMnO_4$ concentration, subject to diffusion of the Mn^{4+} ion. However, the relative emission intensity of the sample first increases and then declines as the $KMnO_4$ concentration is increased, with an optimum $KMnO_4$ concentration of 0.016 g/ml, depending on the concentration quenching effect. The synthesised K_2TiF_6:Mn^{4+} phosphor has excellent thermal stability and was used to produce high-CRI (Ra＞85) white LEDs that are suitable for indoor lighting.

Acknowledgements

This work was financially supported by the National Natural Science Foundation of China (Grant No. 51402032), the China Postdoctoral Science Foundation funded project (Grant No. 2014M562297), the Chongqing Youth Science and Technology talent cultivation project (Grant No. cstc2014kjrc-qnrc40006) and the Chongqing Education Commission funded project (Grant No. KJ1401102).

Notes and references

1 E. F. Schubert and J. K. Kim, *Science*, 2005, **308**, 1274-1278.
2 S. Pimputkar, J. S. Speck, S. P. DenBaars and S. Nakamura, *Nature Photon*, 2009, **3**, 180-182.
3 C. C. Lin and R. Liu, *J. Phys. Chem. Lett.*, 2011, **2**, 1268-1277.
4 R.J. Xie, N. Hirosaki, Y. Li and T. Takeda, *Materials*, 2010, **3**, 3777-3793.
5 R. J. Xie and N. Hirosaki, *Sci. Technol. Adv. Mater.*, 2007, **8**, 588-600.
6 C. Liao, R. Cao, Z. Ma, Y. Li, G. Dong, K. N. Sharafudeen and J. Qiu, *J. Am. Ceram. Soc.*, 2013, **96**, 3552–3556.
7 Q. Zhou, Y. Zhou, Y. Liu, L. Luo, Z. Wang, J. Peng, J. Yan and M. Wu, *J. Mater. Chem. C*, 2015, **3**, 3055–3059.
8 M. J. Lee, Y. H. Song, Y. L. Song, G. S. Han, H. S. Jung and D. H. Yoon, *Mater. Lett.*, 2015, **141**, 27–30.
9 L. Lv, Z. Chen, G. Liu, S. Huang and Y. Pan, *J. Mater. Chem. C*, 2015, **3**, 1935–1941.
10 X. Li, X. Su, P. Liu, J. Liu, Z. Yao, J. Chen, H. Yao, X. Yu and M. Zhan, *CrystEngComm*, 2015, **17**, 930–936.
11 J. H. Oh, H. Kang, Y. J. Eo and H. K. Park, *J. Mater. Chem. C* 2015, **3**, 607–615.
12 H. Nguyen, C. C. Lin, M. Fang and R. Liu, *J. Mater. Chem. C*, 2014, **2**, 10268–10272.
13 L. Lv, X. Jiang and S. Huang, *J. Mater. Chem. C*, 2014, **2**, 3879–3884.
14 J. Meyer and F. Tappe, Adv. Opt. Mater. 3 (2015) 424–430.
15 H. Zhu, C. C. Lin, W. Luo, S. Shu, Z. Liu, Y. Liu, J. Kong, E. Ma, Y. Cao, R. S. Liu and X. Chen, *Nat. Commun.*, 2014, **5**, 4312.
16 A. A. Setlur, E. V. Radkov, C. S. Henderson, J. Her, A. M. Srivastava, N. Karkada, M. S. Kishore, N. P. Kumar, D.

Aesram, A. Deshpande, B. Kolodin, L. S. Grigorov and U. Happek, *Chem. Mater.*, 2010, **22**, 4076-4082.
17 Y. K. Xu and S. Adachi, *J. Electrochem. Soc.*, 2011, **158**, J58-J65.
18 C. Dong and F. C. Van Veggel, *ACS Nano*, 2009, **3**, 123-130.
19 C. Dong, A. Korinek, B. Blasiak, B. Tomanek and F. C. J. M. Van Veggel, *Chem. Mater.*, 2012, **24**, 1297-1305.
20 T. Arai, Y. Arai, T. Takahashi and S. Adachi, *J. Appl. Phys.*, 2010, **108**, 063506.
21 M. A. Noginov, G. B. Loutts, N. Noginova, S. Hurling and S. Kück, *Phys. Rev. B.*, 2000, **61**, 1884.
22 A. S. Aleksandrovskii, L. N. Bezmaternykh, I. A. Gudim, A. S. Krylov and V. L. Temerov, *Inorg. Mater.*, 2002, **38**, 1032-1034.
23 R. Kasa, Y. Arai, T. Takahashi and S. Adachi, *J. Appl. Phys.*, 2010, **108**, 113503.
24 T. Arai and S. Adachi, *J. Appl. Phys.*, 2011, **110**, 063514.
25 D. Sekiguchi and S. Adachi, *ECS J. Solid State SC*, 2014, **3**, R60-R64.
26 H. W. Nesbitt and D. Banerjee, *Am. Mineral.*, 1998, **83**, 305–315.
27 H. K. Park, J. H. Oh and Y. R. Do, *Opt. Express*, 2012, **20**, 10218–10228.
28 M. G. Brik and A. M. Srivastava, *J. Lumin.*, 2013, **133**, 69-72.
29 M. Kubus, D. Enseling, Jüstel and T. H. Meyer, *J. Lumin.*, 2013, **137**, 88-92.
30 S. T. Tan, X. W. Sun, H. V. Demir and S. P. Den Baars, *IEEE Photon. J*, 2012, **4**, 613-619.
31 S. Bhushan and M. V. Chukichev, *J. Mater. Sci. Lett.*, 1988, **7**, 319-321.
32 S. S. Wang, W. T. Chen, Y. Li, J. Wang, H. S. Sheu and R. S. Liu, *J. Am. Chem. Soc.*, 2013, **135**, 12504–12507.

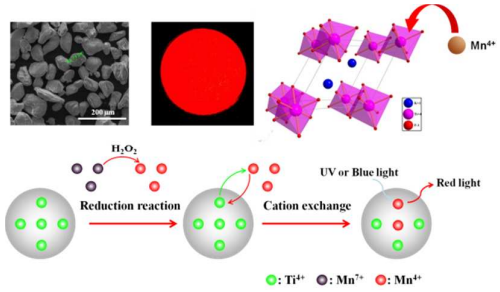

Large micro-sized K_2TiF_6:Mn^{4+} red phosphors synthesised by a simple reduction reaction for high colour-rendering white light-emitting diodes.